Chemosphere 353 (2024) 141463

Contents lists available at ScienceDirect

Chemosphere

journal homepage: www.elsevier.com/locate/chemosphere

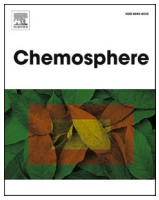

Microplastics role in cell migration and distribution during cancer cell division

Ekaterina Brynzak-Schreiber [a], Elisabeth Schögl [a,b], Carolin Bapp [a], Klaudia Cseh [c], Verena Kopatz [d,e,f,g], Michael A. Jakupec [c], Andreas Weber [b], Tobias Lange [h,i,j], José L. Toca-Herrera [b], Giorgia del Favero [k,l], Wolfgang Wadsak [e,m], Lukas Kenner [d,e,g,n,o,**], Verena Pichler [a,e,*]

[a] University of Vienna, Department of Pharmaceutical Sciences, Division of Pharmaceutical Chemistry, Vienna, Austria
[b] University of Natural Resources and Life Sciences Vienna (BOKU), Department of Bionanosciences, Institute of Biophysics, Vienna, Austria
[c] University of Vienna, Faculty of Chemistry, Institute of Inorganic Chemistry, Vienna, Austria
[d] Medical University of Vienna, Clinical Institute of Pathology, Department for Experimental and Laboratory Animal Pathology, Vienna, Austria
[e] CBmed GmbH – Center for Biomarker Research in Medicine, Graz, Styria, Austria
[f] Department for Radiation Oncology, Medical University of Vienna, Vienna, Austria
[g] Comprehensive Cancer Center, Medical University Vienna, Vienna, Austria
[h] Institute of Anatomy and Experimental Morphology, University Medical Center Hamburg-Eppendorf, Hamburg, Germany
[i] Institute of Anatomy I, Jena University Hospital, Jena, Germany
[j] Comprehensive Cancer Center Central Germany (CCCG), Germany
[k] University of Vienna, Faculty of Chemistry, Department of Food Chemistry and Toxicology, Vienna, Austria
[l] University of Vienna, Faculty of Chemistry, Core Facility Multimodal Imaging, Vienna, Austria
[m] Medical University of Vienna, Department of Biomedical Imaging and Image-guided Therapy, Division of Nuclear Medicine, Vienna, Austria
[n] Unit of Laboratory Animal Pathology, University of Veterinary Medicine Vienna, Vienna, Austria
[o] Christian Doppler Laboratory for Applied Metabolomics, Medical University Vienna, Vienna, Austria

* Corresponding author. University of Vienna, Department of Pharmaceutical Sciences, Division of Pharmaceutical Chemistry, Vienna, Austria.
** Corresponding author. Medical University of Vienna, Clinical Institute of Pathology, Department for Experimental and Laboratory Animal Pathology, Vienna, Austria.
E-mail addresses: lukas.kenner@meduniwien.ac.at (L. Kenner), verena.pichler@univie.ac.at (V. Pichler).

https://doi.org/10.1016/j.chemosphere.2024.141463

Available online 27 February 2024

HIGHLIGHTS

- Plastic particles <1 μm occur within lysosomes of human gastrointestinal cancer cells.
- Microplastic particles accumulate to the non-proliferating areas of tumor spheroids.
- Microplastic particles were transferred between cells during cell division.
- Plastic particles of 0.25 μm increase the propensity for cell migration, and potential for pro-metastatic effects.

GRAPHICAL ABSTRACT

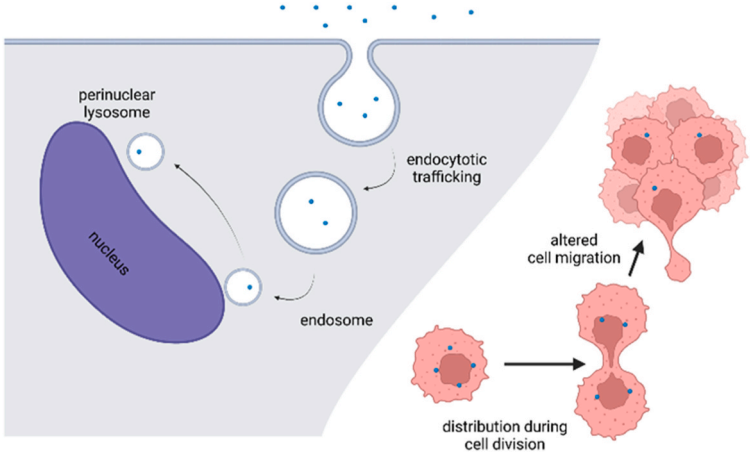

ARTICLE INFO

Handling editor: Michael Bank

Keywords:
Polystyrene
Microplastic
Cell division
Cell migration

ABSTRACT

Amidst the global plastic pollution crisis, the gastrointestinal tract serves as the primary entry point for daily exposure to micro- and nanoplastics. We investigated the complex dynamics between polystyrene micro- and nanoplastics (PS-MNPs) and four distinct human colorectal cancer cell lines (HT29, HCT116, SW480, and SW620). Our findings revealed a significant size- and concentration dependent uptake of 0.25, 1, and 10 μm PS-MNPs across all cell lines, with HCT116 cells exhibiting the highest uptake rates. During cell division, particles were distributed between mother and daughter cells. Interestingly, we observed no signs of elimination from the cells. Short-term exposure to 0.25 μm particles significantly amplified cell migration, potentially leading to pro-metastatic effects. Particles demonstrated high persistence in 2D and 3D cultures, and accumulation in non-proliferating parts of spheroids, without interfering with cell proliferation or division. Our study unveils the disturbing fact of the persistence and bioaccumulation of MNPs in colorectal cancer cell lines, key toxicological traits under REACH (Regulation concerning the Registration, Evaluation, Authorisation and Restriction of Chemicals). Our observations underscore the potential of MNPs as hidden catalysts for tumor progression, particularly through enhancing cell migration and possibly fueling metastasis - a finding that sheds light on a significant and previously underexplored area of concern.

1. Introduction

The gastrointestinal tract (GIT) is daily exposed to substantial quantities of micro- and nanoplastics (MNPs) due to the global increase of plastic pollution. Beyond inhalation, the GIT serves as the primary entry point for MNPs. In 2019, in a pilot study by Schwabl et al. demonstrated the ubiquity of various plastic particles in all examined human stool samples (Schwabl et al., 2019). Subsequent research has illuminated the biodistribution of nanoplastics, in particular, across various organs, (Keinänen et al., 2021; Im et al., 2022) such as the lung, heart and excretory organs, or in the brain (Kopatz et al., 2023). It has been established that the bioactivity of plastic particles is profoundly size-dependent, with nanoparticles exhibiting greater invasiveness and propensity to penetrate cellular membranes. The classification and distinction between MNPs remain contentious, with some definitions demarcating microplastics as 1–1000 μm and nanoplastics as less than 1 μm, (Gigault et al., 2018; Sorensen et al., 2023) while stricter definitions narrow down nanoplastics to below 100 nm (Hartmann et al., 2019). The scientific community is currently engaged in a critical discussion on the feasibility of MNP studies, given the vast heterogeneity of environmental MNPs in terms of chemical composition, form and shape, size and other factors such as biological or chemical corona formation (Brachner et al., 2020).

The internalization of spherical polystyrene (PS) microbeads of sizes 200–1000 nm, 50–100 nm, and 100 nm, respectively, has been demonstrated in human skin fibroblasts (using AFM), (Akhatova et al., 2022) human lung, (Liu et al., 2023) and colon carcinoma cells (D. Xu et al., 2021). Data on other plastic types, such as polyethylene (PE), polypropylene (PP) or polyethyleneterephthalat (PET) which are more prevalent in human exposure, are limited due to difficult production processes of homogeneous and well defined reference material in the micro- and nanometer scale. The dynamic field of MNP research and its recent fast progression resulted in more data on various other plastic types (Annangi et al., 2023; Magrì et al., 2021; Villacorta et al., 2022; Zhang et al., 2022). With the increased availability of different polymer types, our understanding on MNPs and their impact on human health will become more comprehensive. So far, recent evidence suggests that PE and PVC or other particles can also be internalized by human cells, (Cassano et al., 2023) but also mouse embryonic fibroblasts (Barguilla et al., 2022). While plastic particles are known to trigger cellular stress (inducing reactive oxygen species) the mechanisms by which cells or tissues manage accumulated plastic loads remain largely unexplored (Gruber et al., 2022). Given the established presence and potential adverse effects of MNPs, this study specifically aims to explore the role of microplastics in cell migration and distribution during cancer cell division. This focus is crucial for elucidating the broader implications of MNPs on cellular and human health. Although MNPs are highly versatile in their type, shape, composition and undergo different alterations in the environment, PS particles are still a valuable tool to clarify mechanistic issues. Current studies, including the data presented here, are still

limited in investigating all aspects related to MNPs exposure due to the complexity involved in covering all nature of MNPs, additive leaching and corona formation. However, these studies are still valid for clarifying partial aspects of the MNPs toxicological profile.

Plastic particles have long been considered as chemically rather persistent, with the primary mode of degradation being physico-mechanical abrasion (Chamas et al., 2020). Biodegradation of synthetic polymers *via* microbial or enzymatic action is another potential factor, but the high degree of variability makes general predictions of biodegradation challenging and highly dependent on the type of plastic (Mohanan et al., 2020). Cells and tissues have limited capacity to degrade highly persistent and metabolically stable polymer chains found in MNPs *via* both physico-mechanical and biological routes. To our knowledge, degradation routes in humans have not yet been observed, which is crucial for efficient excretion of chemical compounds.

The objective of this study was to 1) investigate the absorption and distribution of polystyrene (PS) particles in colorectal cancer cell lines, including variables such as size, time and concentration; 2) elucidate the uptake mechanism and destination of MNPs once accumulated; and 3) explore the impact of MNPs on cell migration and transfer during cancer cell division. We focused on the direct effects of MNPs on cancerous cells in the gastrointestinal tract, as this is one of the primary tissues exposed to MNPs without the need of the MNPs to cross the intestinal barrier. Elucidating the biological persistence and bioaccumulation of MNPs will significantly impact the perspective of MNPs and their impact on human health. Both factors, persistence and bioaccumulation are included in the toxicological classification of the harmfulness or harmlessness of MNPs under the European Regulation of REACH (Regulation concerning the Registration, Evaluation, Authorisation and Restriction of Chemicals). At this point, further studies are required to investigate long-term accumulation and its effects to create a more holistic view on the behaviour of MNPs for human exposure.

2. Materials and methods

2.1. Materials

All reagents and chemicals were purchased at commercial suppliers and used as received.

3. Polystyrene particles

Commercially available labeled PS particles with a diameter of 10.39 ± 0.13 μm (spherical, aqueous suspension, 5% w/v, blue colored), 1.14 ± 0.03 μm (spherical, aqueous suspension at 2.5% w/v, ex/em = 530/607 nm) and 0.24 ± 0.01 μm (spherical, aqueous suspension at 2.5% w/v, ex/em = 502/518 nm) were obtained from Microparticles GmbH (Berlin, Germany). PS particle characterization was performed measuring ζ potential, size and polydispersity index (PDI) on a Zetasizer Pro device (Malvern Pananalytical, Malvern, United Kingdom). Data analysis was performed using ZS Xplorer software. ζ potential, size and PDI were measured in deionized (DI) water (conductivity of 0.055 μS cm^{-1}), 1 mM KCl solution, 1:9 and 1:99 diluted Phosphate Buffered saline (PBS) (diluted with DI water), RPMI 1640 Media without phenol red (fully supplemented with 10% FCS, 1% penicillin-streptomycin (P/S) and 2 mM L-glutamine), diluted 1:9 and 1:99 with DI water to reduce ionic strength. For cell culture, stock solution of 1 mg mL^{-1} was prepared in sterile water and stored at 4 °C. Working solution was prepared in Gibco RPMI 1640 Media supplemented with 2 mM L-glutamine, 10% (v/v) FBS and 1% P/S in required concentration and incubated for at least 10 min prior to use. Stock suspensions were vortexed at least 10 min before application to resolve potential storage agglomeration.

3.1. Cell culture

Human colorectal cancer cell lines HT29 (ECACC, Porton Down, UK), HCT116 (DSMZ, Braunschweig, Germany), SW480 (ATCC, Manassas, USA), and SW620 (ATCC) were cultivated in fully supplemented MEM culture medium (10% FBS, 1% P/S, 1% L-glutamine) at 37 °C and 5% CO_2 in a humidified atmosphere.

Monolayer cultures were seeded accordingly to experiment requirements as follows: for cell viability assay, 5×10^3 cells in 96-well plates, for FACS analysis, 1.7×10^5 cells per well in 24-well plates or 4×10^5 cells per well in 6-well plates, for confocal microscopy, μ-Slide 8-well 5×10^3 cells per well, for scratch assay 1.75×10^5 cells per well in 24-well plates.

For spheroid formation, HCT116 cells were seeded on Petri dish lids using the hanging drop method at concentrations of 3×10^3 cells per drop for cell viability and 6×10^3 cells per drop for FACS and confocal microscopy in 10 μL drops (Foty, 2011). After 24 h, the medium was replaced by 10 μL of fresh media; and spheroids were transferred to agarose-coated 96-well plates with 100 μL of fresh media per well. Spheroids were allowed to grow for at least an additional 48 h prior to analysis.

3.2. Cell viability assay

24 h after seeding, HCT116 monolayer and spheroids were treated with MNPs for 72 h in the concentration range 0.16–5 μg mL^{-1} 250 mg of thiazolyl blue tetrazonium bromid (MTT, Merck, St. Louis, Missouri, USA) was dissolved in 50 mL of PBS and stored at 4 °C protected from light. MTT stock solution was diluted 1:7 in culture medium (without FBS) prior to use. The supernatant was aspirated from the plate, and 100 μL of MTT solution was added to each well and incubated for 4 h under general cell culture conditions. The MTT solution was aspirated, and formazan crystals were dissolved in 150 μL of DMSO per well. Plates were analyzed at 550 nm (measurement wavelength) and 690 nm (reference wavelength) using the microplate reader Tecan Infinite® M200 Pro (Männedorf, Switzerland) and iControl software.

3.3. Flow cytometry

Particle accumulation studies were conducted using a BD FACSCanto II (BD Bioscience, New Jersey, USA) and a CytoFLEX S (Beckmann Coulter GmbH, Vienna, Austria) flow cytometer. Analysis of cell cycle, particle accumulation in spheroids, and cellular uptake at 4 °C were performed with a Millipore Guava easyCyteTM 8HT flow cytometer (Merck Millipore, Burlington, MA, USA) with InCyte software. FSC, SSC, PE, and FITC fluorescence were recorded. A total of five thousand events were counted for each experiment. Three independent experiments were performed for each sample. The acquired data were analyzed using FlowJo software version 10.6.1 (TreeStar, Ashland, OR, USA).

3.4. Cell cycle

HCT116 cells were settled for 24 h after seeding and then treated with 1 μg mL^{-1} particles for 24 h. The mass concentration of 1 μg mL^{-1} was chosen based on the previous cell viability tests, where the 1 μg mL^{-1} dose showed minor effects on both 2D and 3D HCT116 cells.

Subsequently, cells were washed with PBS, trypsinized and harvested in culture medium, centrifuged and washed once with PBS. Cells were resuspended in Hypotonic Fluorochrome Solution (HFS, consisting of (0.1% (v/v) Triton X-100, 0.1% (w/v) sodium citrate in PBS) and propidium iodide (PI, concentration of 50 mg mL^{-1}) incubated over night at 4 °C. Five thousand events were measured in the flow cytometer.

3.5. Cellular accumulation in 2D and 3D cell culture

For short-term accumulation, cells were allowed to grow for 48 h in 6-well plates. The medium was removed, cells were washed with 1.5 mL PBS per well, and incubated with fluorescent labeled 0.25 and 1 μm PS particles. The cells were exposed to concentrations of 0.1, 1, and 10 μg

mL^{-1} for 24 h and at a concentration of 1 μg mL^{-1} for 1, 3, and 6 h. The mass concentration of 1 μg mL^{-1} was chosen as higher particle concentration showed significant amounts of fluorescence activity limiting the quality of the confocal microscopy images. After the respective incubation period, the cells were washed three times with 1.5 mL of PBS per well and detached by trypsinization with 0.5 mL of Gibco TrypLE Express (Thermo Fisher Scientific, Waltham, Massachusetts, USA) per well. Cells were washed and suspended in 1.5 mL PBS per well and centrifuged (1200 rpm) for 5 min. After centrifugation, the supernatant was discarded and the cell pellet was resuspended in 1 mL of 4% paraformaldehyde (PFA). Cells were fixed for 10 min at room temperature, and centrifuged for 5 min at 1200 rpm. The cell pellet was washed and resuspended in PBS. After another centrifugation step, PBS was removed and the cell pellet was resuspended in FACS buffer consisting of 1% bovine serum albumin (BSA) in PBS and measured.

For medium-term accumulation, cell monolayers were treated with 1 μg mL^{-1} particles for up to 7 d. Spheroids were seeded with 1 μg mL^{-1} particles as hanging drop culture and were allowed to grow for 3–7 d. To provide comparable settings for 2D and 3D conditions, the cells were exposed to the particle solutions once and the cell number was adjusted so that no media exchange was required within the 7 d timeframe. FACS analysis was performed on days 3 and 7 for both cell monolayer and spheroid culture. Cell monolayers were harvested in media, washed with 1× PBS and measured directly in PBS. Ten spheroids at day 3 and five spheroids at day 7 were trypsinized with Gibco TrypLE Express (Thermo Fisher Scientific, Waltham, Massachusetts, USA) in an Eppendorf tube, washed with PBS, resuspended and measured in PBS.

3.6. MNP uptake at 4 °C

Uptake mechanism studies were performed only in monolayer cell culture. HCT116 were seeded in two 12-well plates and allowed to adhere for 24 h. One plate was placed in the refrigerator with chilled medium (approx.15 min), while the other plate remained at 37 °C. Both plates were treated with 1 μg ml^{-1} of 0.25 μm particles for 3 h, cells were harvested, washed once with PBS and FACS measurements were performed.

3.7. Fluorescence measurement and confocal microscopy

3.7.1. Cellular accumulation in 2D and 3D cell culture

Cell imaging was used for analysis of particle uptake and particle localization respectively, using both an inverted fluorescence microscope (Nikon Eclipse TE2000-S) and a confocal laser scanning microscope (Leica TCS SP8-STED and Zeiss LSM 800). HT29, HCT116, SW480 and SW620 cells were exposed to 0.25, 1, and 10 μm particles in concentration of 0.001, 0.01, 0.1, 1, and 10 μg mL^{-1} over the period of 24 h.

3.7.2. Lysosome tracking

LysoTracker® Deep Red (Invitrogen™, Thermo Fisher Scientific, Waltham, Massachusetts, USA, 1:20 dilution) was added to cell monolayers and incubated for 1 h at standard cell culture conditions. Samples were washed thrice with PBS and fixed with 4% PFA in PBS for 10 min at room temperature. After washing the samples thrice with PBS, Hoechst33342 (Invitrogen, Thermo Fisher Scientific, Waltham, Massachusetts, USA) at a dilution of 1:1000 in 1% BSA/PBS was added and samples were incubated for 1 h at room temperature protected from light. Cells were washed with PBS three times and covered with mounting medium (Ibidi GmbH, Gräfeling, Germany) to enable storage. Samples were imaged using the TCS SP8-STED confocal microscope (40× oil objective) and Z-stacks were taken with a step size of 0.3–0.35 μm (software LAS X).

3.7.3. Endosome tracking using EEA1 protein

Cell monolayers were fixed with 4% PFA in PBS for 10 min and washed with PBS three times. Cells were permeabilized with 0.1% TritonX in PBS for 15 min and washed two times with PBS. After blocking with 2% BSA/PBS for 1 h at room temperature, samples were washed two times with PBS. Rabbit anti-EEA1 antibody (Cell Signaling, Danvers, Massachusetts, USA, #2411) was used at a dilution of 1:100 in 1% BSA/PBS for endosome detection, samples were incubated overnight at 4 °C and washed three times with PBS. Goat anti-rabbit IgG (H + L) Alexa Flour 633 (Invitrogen, Thermo Fisher Scientific, Waltham, Massachusetts, USA, A-21070) secondary antibody at a dilution of 1:500 in 1% BSA/PBS and Hoechst 33,342 at a dilution of 1:1000 were added to the sample for 1 h at room temperature, protected from light. Afterwards, cells were washed three times with PBS and covered with mounting medium to enable storage. Samples were imaged using the TCS SP8-STED confocal microscope (40× oil objective) and Z-stacks were taken with a step size of 0.3–0.35 μm (software LAS X).

3.7.4. Proliferation assessment by Ki67

Untreated and treated spheroids (1 μg mL^{-1}) were embedded in Tissue-Tek O.C.T. Compound (Sakura) on day 3 and 7, and 7.5 μm thick cryosections were prepared on Superfrost™ microscope slides (Epredia) using a Leica CM3050 S cryomicrotome and stored at −80 °C. The samples were fixed with 4% PFA in PBS for 20 min and washed with PBS three times. Cells were permeabilized with 0.1% TritonX in PBS for 10 min and washed two times with PBS. Blocking was performed with goat serum (PBS + 10% goat serum + 2% BSA) for 1 h and samples were washed two times with PBS. Primary antibody Ki67 (8D5) mouse mAb (Cell Signaling, 9449S) was applied in 1:800 dilution in 2% BSA/PBS, and samples were incubated over night at 4 °C. After washing with PBS for three times, secondary antibodies anti-mouse IgG H&L (Alexa Flour488, Abcam, 4408S) and anti-mouse IgG Fab2 (Alexa Flour 647, Abcam, 4410S) were added at a dilution of 1:1000 in 2% BSA/PBS and samples were incubated for 1 h at room temperature. Finally, three drops of ProLong® Gold antifade reagent (Thermo Fischer Scientific) with DAPI were added and slides were covered by cover slips. Samples were dried overnight and analyzed on the next day with a Zeiss LSM 800 (10× and 20× objective).

3.7.5. DiO assessment of endocytic trafficking

5×10^3 cells per well were seeded and treated immediately with 1 μg mL^{-1} particles in μ-Slide 8-well chamber slides using Gibco FluoroBrite™DMEM (Thermo Fisher Scientific, Waltham, Massachusetts, USA), supplemented with 2 mM L-glutamine, 10% (v/v) FBS and 1% P/S and allowed to attach for 24 h. Cells were stained with 3 μM DIO (3,3′-dioctadecyloxacarbocyanine perchlorate) in PBS for 15 min. Stained samples were washed three times with PBS and monitored in FluoroBrite™DMEM with a Zeiss LSM 800 (63× oil objective) maintaining growth conditions with an XLmultiS incubator. Images were taken every 10 min for a maximum of 4 h per area during an overall incubation time of 24 h.

3.7.6. Live imaging of cell division

Cells were seeded in μ-Slide 8 well chamber slides using FluoroBrite™DMEM supplemented with 2 mM L-glutamine, 10% (v/v) FBS and 1% P/S, treated with 1 μg mL^{-1} PS particles, and monitored for 24–48 h with a Zeiss LSM 800 (20× objective) maintaining growth conditions with an XLmultiS incubator. Samples were stained with 5 μM Hoechst 33,342 solution for 15 min. Colocalization was analyzed by ImageJ v1.54f software. Cell migration and trajectory was analyzed by Fiji/ImageJ applying the TrackMate plugin (Ershov et al., 2022).

3.7.7. Cell migration assay

HCT116 cells were seeded in 24-well plates in medium containing 1 μg mL^{-1} MNPs and incubated for 48 h. Further 1 μg mL^{-1} particles were added, the confluent cell layer was scratched with a sterile 200 μL pipet tip, and cell migration was monitored for 48 h with a JuLI Br system (NanoEnTek) simultaneously for negative control and treated sample. Data were analyzed using JuLI Br software.

4. Statistics

All experiments were performed at least in duplicate and repeated three times if not indicated otherwise. Untreated controls without particles were included in each experiment. All values are given as mean ± standard deviation (SD). Analysis of data was performed either with MS Excel or GraphPadPrism9. Significance tests were performed with GraphPadPrism9. Flow cytometry data were evaluated using Flowing Software 2 (Turku Bioscience, University of Turku and Åbo Akademie University, Turku, Finland, 2013) or FlowJo™ Software version 10.7 BD.

5. Results

5.1. Polystyrene particle characterization

The commercially available PS particles were characterized by ζ potential, size, shape and polydispersity index (PDI) as a measure for potential aggregation (SI Table 1) in comparison to the data provided by the manufacturer. The particles were measured in DI water, 1 mM KCl, (see SI Table 1) and diluted PBS as well as diluted cell culture medium with FBS (data not shown). Data for the measurements in fully supplemented cell culture medium are not shown due to controversies in literature (Bhattacharjee, 2016).

Particle size in DI water correlated with the manufacturer's results. An increase in salt concentration led to an increase in particle size due to a different hydrodynamic radius related to the higher ion concentration. Due to the variability in size and ζ potential depending on the suspension media, we will refer to the particle size more generally as 0.25, 1 and 10 μm. Particle aggregation was not observed in DI water and 1 mM KCl suspension. However, aggregation, particularly of the 0.25 μm particles, was observed when exposed to cell culture media with FBS. To minimize potential aggregation, particle solutions were vortexed for 10 min prior to cell treatment.

5.2. Cell viability and effect on cell cycle

In a first step, effects of characterized MNPs on HCT116 cell viability in monolayer and spheroid culture were assessed over a period of 72 h in a concentration range of 0.16–5 μg mL^{-1}. The results should facilitate dose-finding for subsequent experiments. We could detect a significant detrimental effect of the tested MNPs on cell viability in monolayer culture in a dose- and size-dependent way (Fig. 1A), while spheroids were more resistant to MNPs (Fig. 1B). In general, smaller particles had a more pronounced effect than the 10 μm particles. This result correlates with previous findings, indicating that bigger particles are less harmful than smaller ones (Ding et al., 2020). Subsequently, we focused primarily on smaller particles and an intermediate concentration of 1 μg mL^{-1} for the following experiments, if not otherwise stated. The concentration of 1 μg mL^{-1} was chosen, as at this concentration an excellent balance between accumulation and fluorescence signal was achieved (SI Figs. 1–3) while remaining in a physiological relevant low dose of particles. HCT116 monolayers were exposed to 1 μg mL^{-1} of PS particles of 0.25 or 1 μm to investigate potential effects on the cell cycle after 24 h (Fig. 1C). Exposure of HCT116 cells to 0.25 μm particles did not alter their distribution across cell cycle phases during this short-term experiment (Fig. 1C).

5.3. Short and medium term cellular accumulation studies

HT29, HCT116, SW480, and SW620 cell monolayers were treated with 0.25, 1, and 10 μm particles in concentrations ranging from 0.001 to 10 μg mL^{-1} and uptake of the particles was monitored for 24 h using fluorescence microscopy (SI Fig. 1). Intracellular uptake of 1 μg mL^{-1} of 0.25 μm and 1 μm particles was additionally confirmed through FACS measurements over four different time points (Fig. 2A and B). Overall particle accumulation varied significantly depending on particle size, time, concentration, and cell line. 0.25 and 1 μm particles were found to be closely associated to cellular membranes and were taken up by all cell lines, while 10 μm particles were distributed around the cells, not attached to the cell layers, and could be removed by washing with PBS or

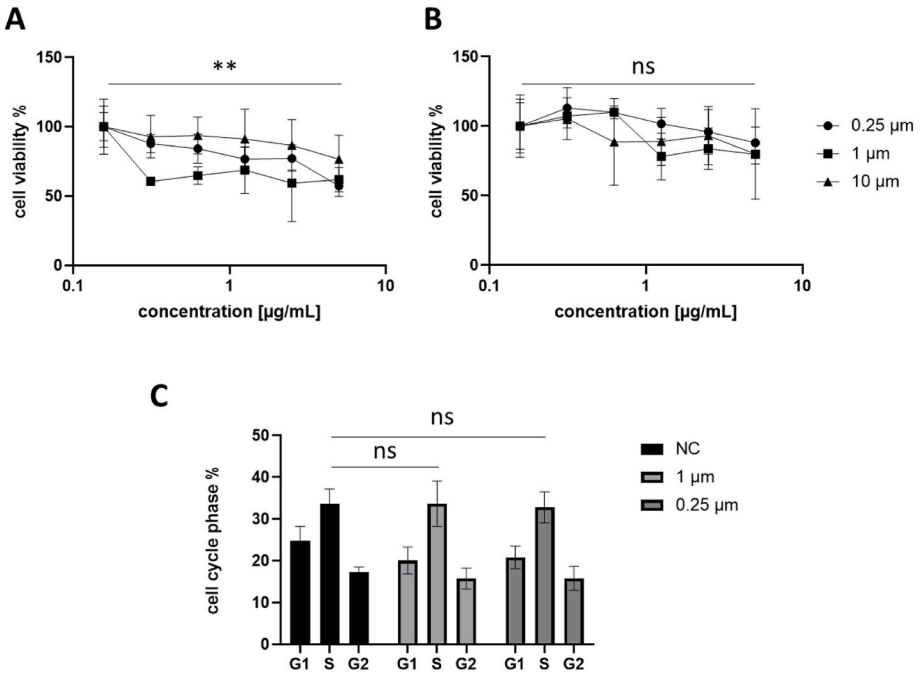

Fig. 1. Cell viability in monolayer and spheroid culture and effects on cell cycle. **(A)** Dose-response curves of HCT116 monolayer cells and **(B)** HCT116 multicellular tumor spheroid exposed to increased mass concentration of MNPs with particle sizes of approx. 0.25, 1, and 10 μm over an incubation time of 72 h by means of MTT assay. Significance is depicted for 0.25 μm particles compared to the control. **(C)** FACS analysis of the cell cycle of HCT116 monolayer cells without MNPs and exposed to 1 μg mL^{-1} of 0.25 and 1 μm particles.

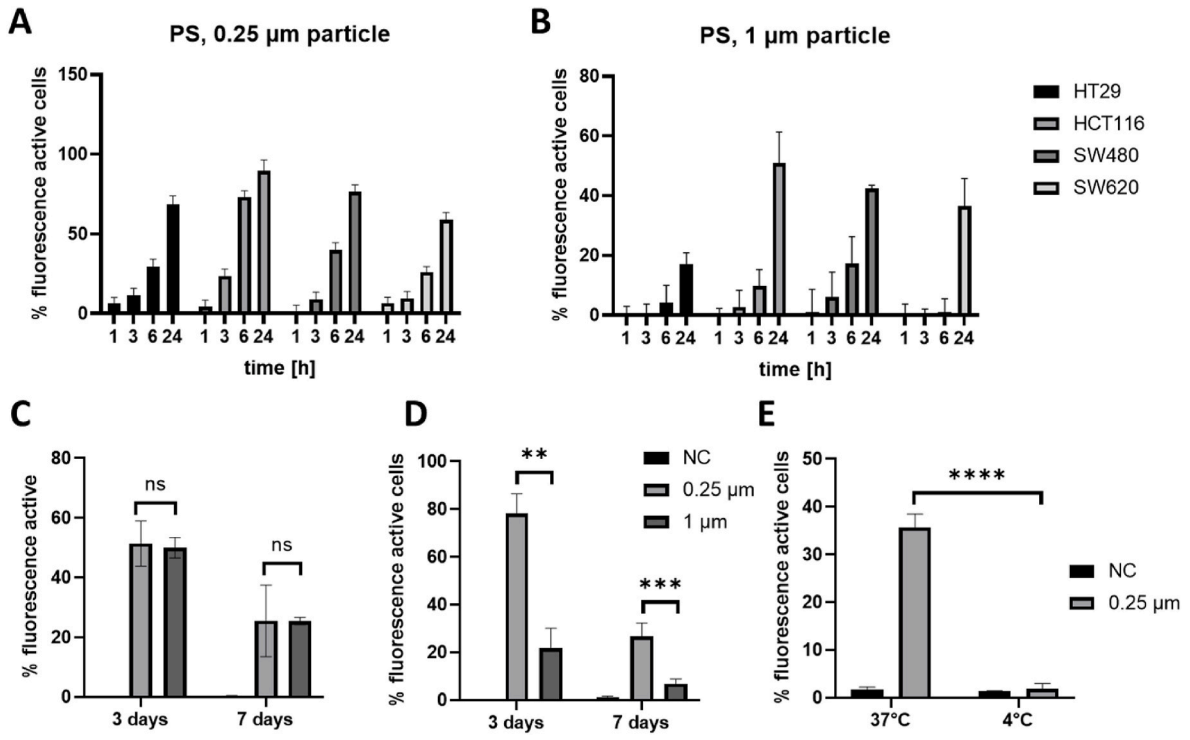

Fig. 2. Uptake of 0.25 µm and 1 µm PS particles in monolayer and spheroid culture in colon cancer cell lines treated with 1 µg/mL. The percentage of particle-positive cells over the total cell population in comparison to negative control (NC) is presented for **(A)** 0.25 µm and **(B)** for 1 µm particles in four different colorectal cancer cell lines and for four different time points. Data are shown as means ± standard deviation (SD), $n = 2$. **(C)** Uptake of 0.25 µm and 1 µm particles in HCT116 monolayer culture. **(D)** Uptake of 0.25 µm and 1 µm particles in HCT116 spheroid culture. **(E)** Uptake mechanism studies. HCT116 were incubated with 1 µg mL^{-1} of 0.25 µm particles at 37 °C and 4 °C, and uptake measured after 3 h. Data are shown as means ± standard deviation (SD), $n = 3$–5. *T*-test results shown above.

culture medium (data not shown).

Increasing the incubation time resulted in increased accumulation of 0.25 µm and 1 µm particles in all tested colorectal cancer cell lines, with faster intracellular presence observed for 0.25 µm particles compared to 1 µm particles. The enhanced uptake of smaller particles was indicated by the fact that 0.25 µm particles were notably present in all tested cell lines already after 6 h of incubation while it took 24 h for 1 µm particles to become detectable in all tested cell lines (Fig. 2A and B). The efficacy of particle interaction and accumulation with the cells were strongly cell line-dependent in the following increasing order for 1 µm after 24 h: HT29 < SW620 < SW489 < HCT116, indicating HCT116 cells as most efficiently involved in particle interactions. Within 6 h, 73.2% of HCT116 cells treated with 0.25 µm particles exhibited green fluorescence, reaching 89.5% after 24 h.

Cell populations with different numbers of internalized 0.25 µm and 1 µm *PS* particles were identified for all cell lines using flow cytometry. Kinetic analyses at three different time points with fixed PS concentration of 1 µg mL^{-1} (SI Fig. 2) as well as concentration dependency with three different particle concentrations at a fixed time point of 24 h (SI Fig. 3) were performed. In general, the absolute number of particles accumulated within the cell was clearly assessable for 1 µm *PS* particles out of the FACS histogram curves, whereas 0.25 µm particles resulted in a bell-shaped histogram. For 1 µm particles, after 1–6 h mainly one particle was internalized per cell. After 24 h, 12.37, 10.83 and 3.21% of HCT116, SW480, and SW620 cells had taken up more than four particles per cell, respectively, and 4.14% of HT29 cells more than 3 particles per cell. Increasing concentration led to an increase in particle uptake(SI Fig. 3). In general, intracellular 1 µm particles exhibited double-positive signals, while 0.25 µm particles were only active in the green channel (SI Fig. 4). Based on these results, we have chosen an incubation time point of 24 h for all further short-term measurements.

Only HCT116 cells and a concentration of 1 µg mL^{-1} were chosen for further medium-term analysis in monolayer and spheroid culture over a period of 7 d. HCT116 cells were chosen as these cells had the highest accumulation rate and therefore facilitate distribution and accumulation studies. An intermediate concentration of 1 µg mL^{-1} was applied to avoid imaging interferences occurring at 10 µg mL^{-1} due to the high fluorescence activity of the particles. HCT116 multicellular spheroids were formed with the hanging drop method and analyzed at the same time points, expecting the spheroid formation to be fully completed on day 3 and the core to become profoundly necrotic till day 7 (Hirschhaeuser et al., 2010; Sutherland, 1988). It should be noted that ultra-low attachment plates and agarose-coated plates did not lead to particle accumulation within the spheroid, as high adsorption of the plastic particles to the plastic surface was observed (data not shown). The hanging-drop formation method was preferred to minimize the interaction of the fluorescently labeled particles with the plastic of the cell culture material.

PS particles of sizes 0.25 and 1 µm were found intracellularly even after 7 d of incubation, although the proportion of particle-positive cells detected by FACS was lower compared to day 3. In monolayers, the uptake efficacy of 0.25 µm and 1 µm particles was comparable to day 3, reaching approximately 50% of the total cell population. However, in spheroid culture, 0.25 µm particles exhibited accumulation rates at least four times higher than 1 µm particles on both day 3 and day 7 (Fig. 2C and D). Furthermore, both particle sizes demonstrated a significant decrease in fluorescent signal over time in both spheroids and monolayers, indicating a decrease in particle numbers relative to the total cell number due to cell proliferation. This decrease can primarily be attributed to the experimental conditions where cell numbers increased over time due to cell proliferation, while the particle count remained constant throughout the incubation period. Particles with a size of 0.25 µm exhibited significantly higher uptake rates in spheroids compared to monolayer cultures, whereas particles measuring 1 µm demonstrated significantly higher uptake in monolayer cultures than in spheroids. The 1 µm particles exhibited double positive signals, while 0.25 µm particles

were only active in the green channel(SI Fig. 6).

5.4. Cellular uptake mechanism studies

To evaluate possible routes of particle uptake, the active transport mechanism was suppressed under hypothermic conditions during the exposure of HCT116 monolayers to 1 μg mL^{-1} of 0.25 μm particles (Fig. 2E). Under these conditions, active uptake of 0.25 μm was inhibited to the level of non-treated control while the uptake rates under normal conditions were at 37% particle positive cells after 3 h, confirming that the employed polystyrene particles were actively transported into HCT116 cells. A similar active transportation was reported for human lung cells (Liu et al., 2023). Colocalization of PS particles with formed vesicles was observed by applying DiO membrane dye to visualize the endocytic mechanism of MNP accumulation. The lipophilic fluorescent dye DiO serves as a general membrane and vesicle stain (Martens et al., 2014).

Real-time imaging was employed to visualize the uptake process in each region for a maximum of 4 h, contributing to an overall observation period of 24 h (Fig. 3; SI Video 1). Colocalization analysis was challenging due to the overlapping excitation and emission spectra of the fluorescent particles. Additional counterstaining of fixed cells was performed with DAPI to visualize the nucleus. DiO colocalization studies showed that 1 μm MNP particles were trapped intracellularly and exhibited a high degree of colocalization with formed vesicles, confirming the internalization of the PS particles *via* endocytosis. As seen in previous experiments, particles also accumulated in the peri-nuclear region.

Supplementary video related to this article can be found at https://doi.org/10.1016/j.chemosphere.2024.141463

5.5. Localization and distribution

After confirming active transportation, the behavior of the MNPs was analyzed over time to investigate their accumulation and distribution. The localization and distribution of the particles were studied in both monolayer and spheroid culture to clarify intra- and extracellular allocation. Organelle staining was performed to evaluate the localization of incorporated particles within the cells. In living cell monolayers and spheroids of the HCT116 colon cancer cell line treated with 0.25 μm and 1 μm particles, the nuclei were stained with Hoechst 3342. Confocal laser scanning microscopy was used to capture images at different time points and orthogonal projections. Three-dimensional images of the Z-stacks were created. These images indicated close colocalization of both particle sizes in the peri-nuclear region (SI Fig. 5). This is in accordance with the fact that PS particles of different sizes can enter macrophages and other cell types *via* the endocytosis pathway and interact with the endosomal-lysosomal system (Chang et al., 2020; Fröhlich et al., 2012). Furthermore, we hypothesized that incorporated particles would be detectable as a color change of stained lysosomes or endosomes from red to yellow. To test this hypothesis, HT29, HCT116, SW480, and SW620 cell lines grown in monolayers were exposed to 1 μg mL^{-1} of fluorescent 0.25 μm and 1 μm particles for 24 h. Fixed cell monolayers were stained with LysoTracker Deep Red (red) to visualize lysosomes, and a primary EEA1 antibody and an Alexa Fluor 633-conjugated secondary antibody were used to stain endosomes (red). The stained samples were then monitored using confocal laser scanning microscopy (Fig. 4).

0.25 μm PS particles showed strong colocalization with endosomes (Fig. 4A) and lysosomes (Fig. 4B) in all four cell lines, their overlap yielding a yellow fluorescence signal. Internalization and colocalization with endosomes and lysosomes were confirmed by Z-stack imaging. Although 1 μm PS particles were found in lysosomes of all four tested cell lines (SI Fig. 5), only HCT116 endosomes seemed to incorporate this size of particles.

To gain insight in particle distribution and localization in tissues, multicellular spheroids of the HCT116 colon cancer cell line were co-incubated with 1 μg mL^{-1} of 0.25 μm and 1 μm PS particles during the spheroid formation process. Live spheroids were monitored by confocal microscopy and Z-stack imaging at day 3 and 7 (data not shown). As previously demonstrated in FACS experiments, the particles were found both intra- and extracellularly in the formed spheroids after 3 and 7 d (Fig. 3).

Ki67 as a sensitive proliferation marker was used for proliferation studies in multicellular spheroids. Staining on day 3 and 7 showed comparable expression levels of Ki67 in treated and untreated samples (SI Video 2 + 3). Due to limitations of the confocal microscope of larger spheroids at day 7 and to ensure better orientation within the cell layers and spheroid zones,(Ware et al., 2016) spheroids were cryo-sectioned at day 3 and 7 and stained with Ki67 and DAPI. Both 1 and 0.25 μm particles showed strong colocalization with the necrotic core in 7-days old spheroids, while in 3-days old spheroids distribution was again quite uniform (Fig. 5). While the concentration of particles in the inner zones of the spheroid still appeared high, fewer particles were found in the proliferation zone. This indicates that proliferating cells either excrete the particles or, more likely, redistribute the particles during cell division leading to decreased signals. In order to be able to follow the redistribution of the MNPs, no new MNPs were added during the experiment. We investigated this possibility by performing live cell imaging, monitoring the cell division of cells with incorporated PS particles over a 2-h period (Fig. 6). Cell division was monitored as brightfield and fluorescence overlay image, as well as counterstained with DAPI to visualize the nuclei. Both particle sizes were distributed between daughter cells during cell division (Fig. 6, SI Video 4). No excretion was observed during the monitored time frame.

Supplementary video related to this article can be found at https://doi.org/10.1016/j.chemosphere.2024.141463

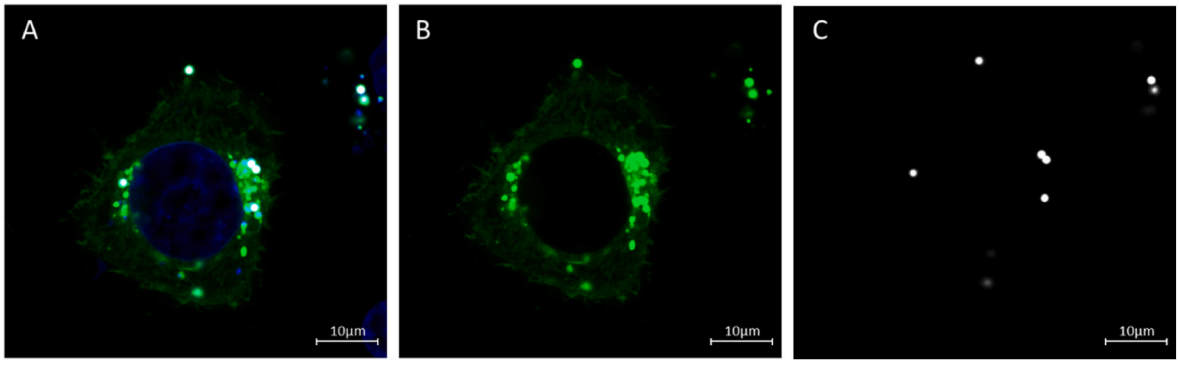

Fig. 3. Vesicular endocytic uptake of PS particles. DiO stain to visualize cell membrane and vesicular endocytic trafficking over the course of 4 h including Hoechst3342 counterstain with DiO incubation after 1 μm particle treatment. **(A)** Overlay of DiO and Hoechst3342 staining and fluorescently-labeled 1 μm particles. **(B)** Single channel analysis of DiO staining of cellular membrane and vesicle formation and **(F)** single channel analysis of particle fluorescence.

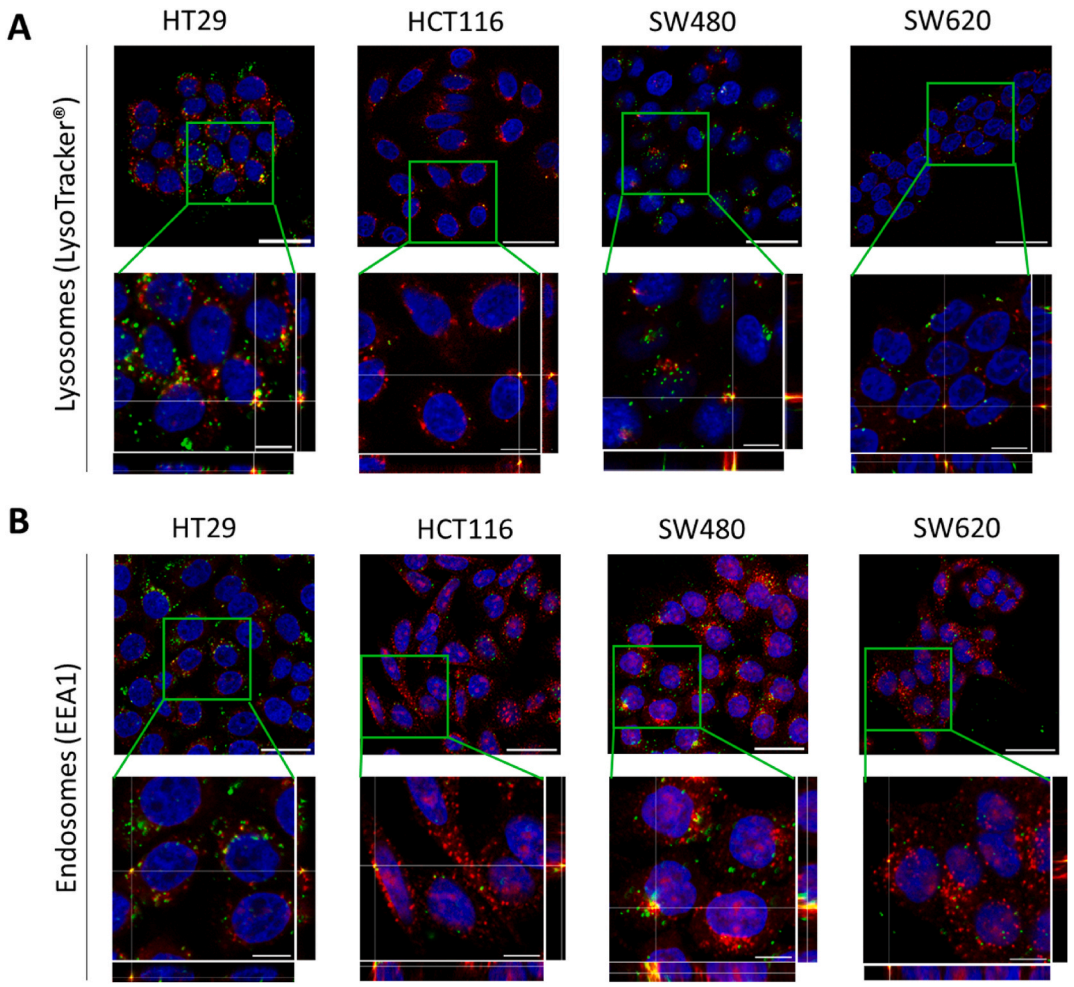

Fig. 4. Cellular internalization and localization of 0.25 μm PS particles in endosomes (A) and lysosomes (B). HT29, HCT116, SW480 and SW620 cells exposed to 1 μg mL^{-1} 0.25 μm PS particles for 24 h. CLSM images on top represent an overview of the cell population at 40× magnification, while images below correspond to the zoomed area (with orthogonal projections of Z-stacks), of the indicated green squares in the original picture. Nuclei are stained in blue, endosomes **(A)** or lysosomes **(B)** in red and 0.25 μm PS particles appear in green. Yellow is the merged fluorescence of PS particles and endosomes or lysosomes. Scale bars: 30 μm. (For interpretation of the references to color in this figure legend, the reader is referred to the Web version of this article.)

5.6. Cell migration and wound healing

Live imaging not only enables investigations on cell division, but also facilitates the visualization of cell migration and the trajectory of each cell. Based on initial analysis of the live cell imaging (see SI Fig. 7), we wanted to further investigate potential differences in cell migration *via* a more well-established assay like the scratch assay. Cell migration is the initial step in metastasis formation and therefore one of the characteristics for cancer aggressiveness and disease progression (Gerashchenko et al., 2019; Novikov et al., 2021). Exposure to microplastics has been shown to induce actin cytoskeleton rearrangements in epithelial cells (Yanting Li et al., 2022a). We hypothesized that the impact on the cytoskeleton might have an effect on cell migration too and used a scratch assay to investigate possible effects triggered by MNP exposure. HCT116 cells were treated with 1 μg mL^{-1} of PS particles for 48 h prior to the scratch and again with 1 μg mL^{-1} prior to the 24 h monitoring of the wound healing process. After only 12 h, an effect was visible for both particle sizes. 0.25 μm particles significantly increased cell migration speed compared to untreated control, while 1 μm particles had only a minor effect decreasing the propensity for cell migration (Fig. 7), highlighting the size-dependent effects of PS particles.

6. Discussion

The omnipresence of plastic in our society and environment inevitably leads to human exposure. MNP contamination of food is particularly concerning, as the GIT is likely the first site of daily exposure to MNPs (Schwarzfischer et al., 2022). This study aimed to investigate the interaction between different PS-MNP and colon cancer cell lines, focusing on the influence of particle size on cellular internalization, the localization of MNP in cellular compartments, and their accumulation and distribution in a more complex spheroid model. Absorption and distribution are two of the major aspects of toxicokinetics determining the fate of ingested and accumulated compounds. In our study, we focused on MNPs directly accumulated in gastrointestinal cancer cells, which are exposed to MNPs without the need to cross the intestinal barrier and spread through out the organism. Further experiments and other well-established in vitro models would be required to study MNPs effect on the intestinal barrier. We selected four different colon cancer cell lines to represent a model of cancer progression and to investigate whether the aggressiveness of the respective cell line impacts particle uptake and distribution, as well as cell division and migration. Prior to MNP exposure, the particles were meticulously characterized for their physico-chemical parameters. Although measured, the ζ-potential obtained in cell culture medium is not presented, since this data should be interpreted with caution as the complex mixture of additives and protein

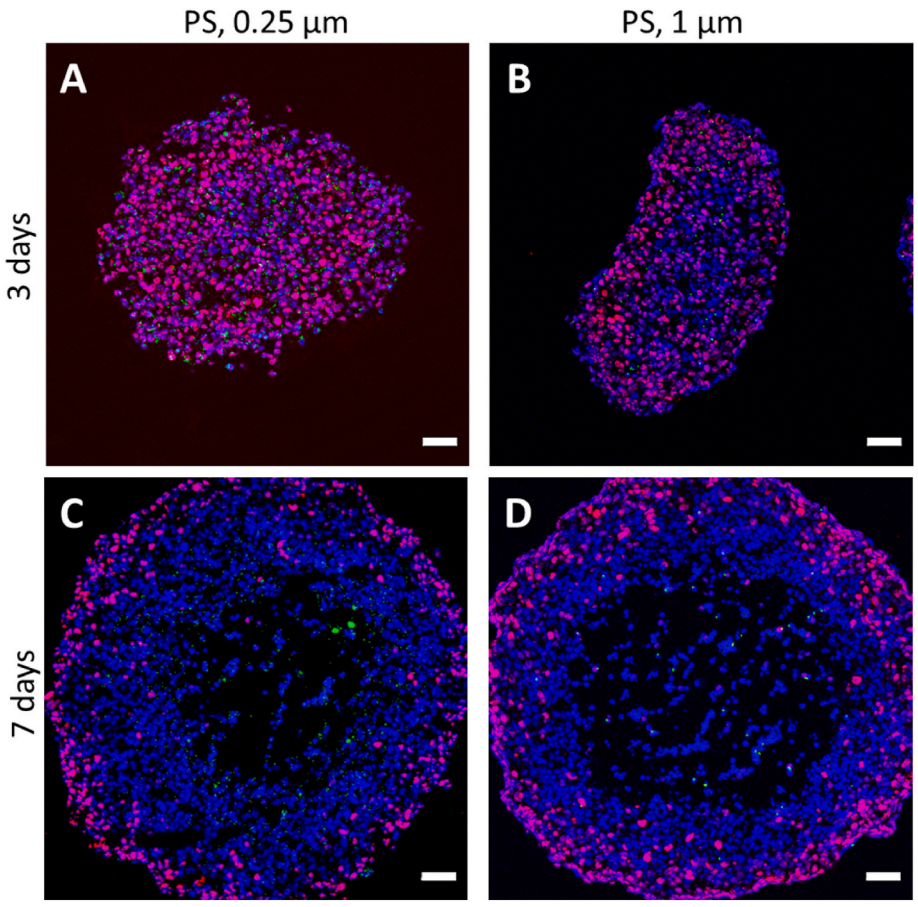

Fig. 5. Distribution of MNPs in multicellular tumor spheroids. CLSM images of HCT116 spheroids formed in presence of 1 µg mL^{-1} of PS particles, stained with Ki67 (magenta) and DAPI (blue). **(A,C)** 0.25 µm PS particles, spheroids at day 3 and 7, respectively, **(B,D)** 1 µm PS particles, spheroids at day 3 and 7 respectively. Both particle sizes are shown in green due to better contrast. Images **A** and **B** show equable distribution of incorporated particles, while images **C** and **D** indicate colocalization with the necrotic core of the spheroid, whereas the proliferation zone in pink is in both cases particle free. Scale bars: 50 µm. (For interpretation of the references to color in this figure legend, the reader is referred to the Web version of this article.)

concentration can interfere with the measurement and potentially compromise the validity of the data (Bhattacharjee, 2016). As shown previously, MNPs induce toxicity in different cell types (Yuqi Li et al., 2022b; M. Xu et al., 2019) and even whole organisms (Yong et al., 2020). However, the doses required to induce significant effects on cell viability within this short time period were considerably higher than those found in realistic human settings. It was confirmed that 10 µm particles are less harmful than particles of size 1 µm or smaller, as demonstrated by Stocke et al. (Stock et al., 2019;Zauner et al., 2001; Banerjee et al., 2021)

Short time experiments indicated that exposure to PS particles had no effect on cell proliferation and cell cycle distribution(Hwang et al., 2020; Vecchiotti et al., 2021). Despite the assumption of Bill-Karniely et al.(2020), who hypothesized that more deformable and 'soft' cell types would take up more particles, SW620 cells showed a lower uptake after 24 h for both, 0.25 and 1 µm PS particles, than SW480 cells (Armistead et al., 2020). Since the cell line HT29 is derived from a primary adenocarcinoma with Duke's Stage C and has a similar elastic modulus as SW620, (Armistead et al., 2020) it was assumed that particle uptake in this cell line would be higher than in SW480 cells isolated from a Duke's Stage B primary adenocarcinoma. However, the observations of our study contradict this hypothesis, because after 24 h of incubation HT29 cells showed the lowest uptake of 1 µm PS particles compared to other cell lines. Moreover, also lower uptake rates of 0.25 µm PS particles into HT29 cells were observed compared to SW480 cells. HCT116 cells, on the other hand, showed the highest uptake rates for both 0.25 and 1 µm PS particles. Since there is no uniform classification of the HCT116 cell line in the literature regarding its cancer aggressiveness, it is difficult to relate the results of HCT116 cells to those of other cell lines. The high uptake rates in HCT116 cells could be due to their belonging to the mesenchymal consensus molecular subtype 4 (CMS4), which may be more aggressive due to upregulation of genes involved in epithelial mesenchymal transition (EMT) and signatures related to the activation of transforming growth factor β (TGF*β)* (Guinney et al., 2015).

All four cell lines showed substantial uptake of the 1 µm and especially of the 0.25 µm PS particles, whereas no uptake of the 10 µm particles was observed. This result aligns with previous reports that set the upper limit of intracellular MNP uptake in intestinal epithelial cells at 10 µm (Bruinink et al., 2015). Therefore 10 µm particles were excluded from further studies. In general uptake efficacy was size dependent for all cell lines as indicated elsewhere (Foroozandeh and Aziz, 2018). Biodistribution was further validated in spheroid culture of the HCT116 colon cancer cell line, with 0.25 µm PS particles showing significantly higher intracellular uptake than those of 1 µm. 0.25 µm particles had significantly higher uptake rates in spheroids than in monolayer, while the uptake of 1 µm particles was significantly higher in monolayer than in spheroids. The formation process of spheroids naturally leads to a difference in sedimentation rates between cells and PS particles of different sizes. Generally, cells sediment faster than PS particles.

However, the uptake rates and speed are highly dependent on the uptake mechanism involved. Many possible routes have been identified and dependencies on particle properties and cell line have been underlined previously (Firdessa et al., 2014; Kuhn et al., 2014). It has been shown that uptake of smaller particles (<0.5 µm) is in many cases a

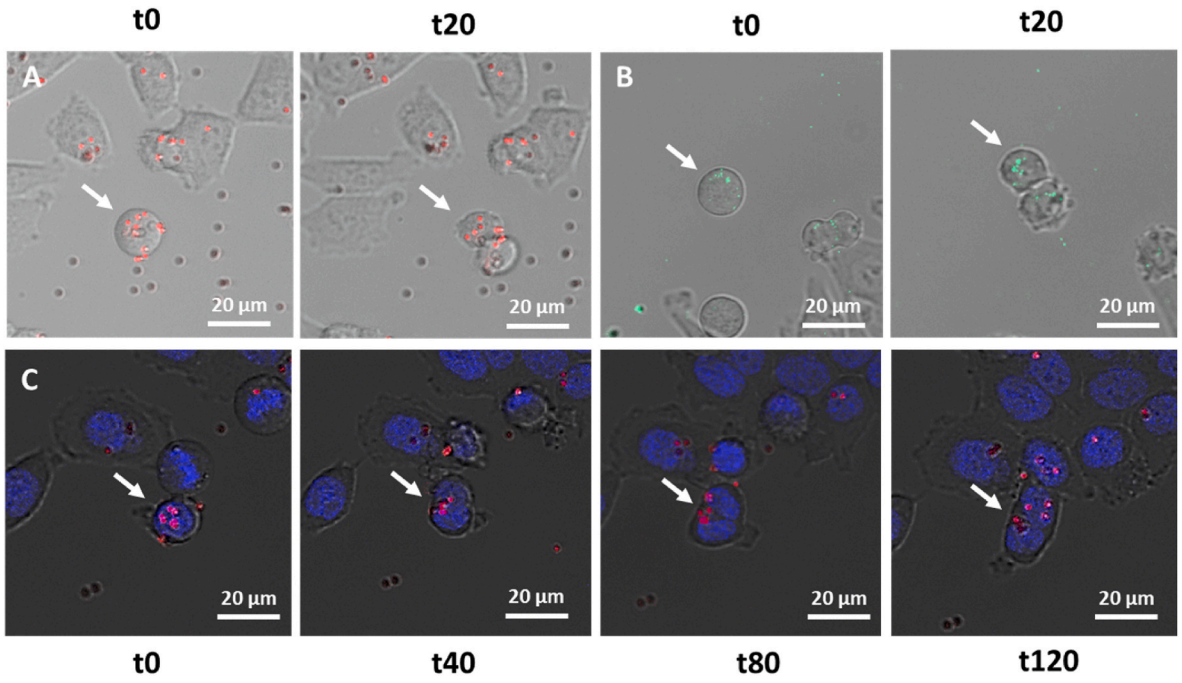

Fig. 6. Distribution of PS particles during the cell division. CLSM images of HCT116 exposed to 1 µg mL^{-1} of **(A)** 1 µm or **(B)** 0.25 µm PS particles. Pictures show particle uptake before and after mitosis (t0 and 20 min later t20). **(C)** Mitosis time-course of HCT116 treated with 1 µg mL^{-1} of 1 µm particles and co-stained with Hoechst 3342. Time-dependent images were recorded every 20 min for a total of 120 min. Scale bars: 20 µm.

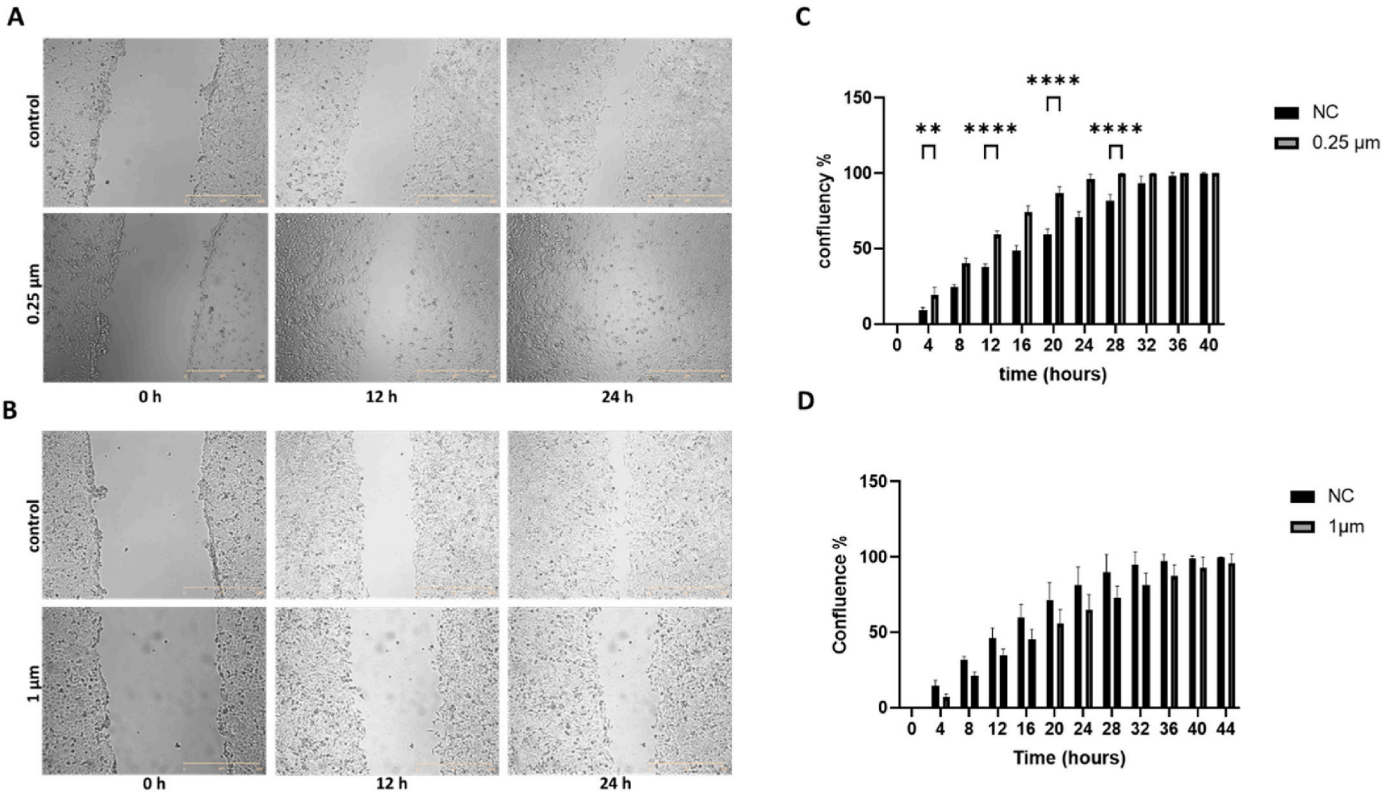

Fig. 7. Scratch assay of HCT116 cells treated with 0.25 and 1 µm particles. Brightfield microscopy of scratch closure of cells treated with **(A)** 0.25 µm and **(B)** 1 µm particles and a particle concentration of 1 µg ml^{-1} compared to negative control (NC) after 0, 12 and 24 h monitored with JuLI BR system. Scratch closure analysis during 48 h of **(C)** 0.25 µm (highly significant) and **(D)** 1 µm particles (non-significant). Significance was calculated using GraphPadPrism and 2-way ANOVA.

receptor mediated process, such as clathrin or caveolin mediated endocytosis, while lager particles (>0.5 µm) are taken up through phagocytosis or micropinocytosis(Foroozandeh and Aziz, 2018). Consistent with the fact that clathrin and caveolin mediated endocytosis causes formation of early and late endosomes, which than fuse with lysosomes, 0.25 µm particles could be identified both in endosomes and

lysosomes of all tested cell lines, while 1 μm particles were not observed in endosomes. It might be speculated that 1 μm particles were taken up by phagocytosis in most of the tested cell lines, as some of the cancer cell lines are capable of phagocytosis, (Ghoneum and Gollapudi, 2004) which may explain why they were mostly detected in lysosomes. HCT116 cells could, however, have additional uptake routes such as micropinocytosis which is an endosome mediated process.

In spheroid culture particle of both sizes were colocalized with the necrotic core in 7-days old spheroids while the proliferation zone remained particle free. During the growth phase of the spheroid, we refrained from adding additional MNPs to media, as we wanted to study how the tissue response to once accumulated MNP. Continuous addition of MNPs would not allow us to identify the movement of once accumulated MNPs in tissue. However, our studies showed a redistribution of the MNPs within the spheroid, starting from a uniform distribution on day 7, to an irregular distribution with lower MNPs concentration in the proliferation zone and higher MNPs in the necrotic zone. These observations could be explained by distribution of PS particles between the daughter cell during cell division, therefore non proliferating cells had higher particle values after 7 d, while strongly proliferative cells in the periphery had no detectable signal or reached the limit of detection. To the best of our knowledge, we were the first to show the fate of incorporated particles during cell division. Remarkably, short exposure of 0.25 μm particles significantly increased the propensity for migration of the cells, indicating possible pro-metastatic effects, that should be evaluated further on gen regulation and functional levels. 1 μm particles, in contrast, had no significant impact on cell migration, again underlining size dependency. However, MNPs are expected to cause chronical toxicity and have been shown to do so in various organisms, (Gonçalves et al., 2022; Sobhani et al., 2021) therefore, long-term experiments should evaluate further effects.

One of the major limitations of the study is the accessibility of particles with defined other shapes, which more closely resembles the abrasion and degradation processes in the environment. Moreover, we need more data on chronic exposure of more realistic particles to clarify if toxic effects occur. The global strategy for evaluating and ensuring chemical safety is based on the assessment of persistence (P), bioaccumulation (B), and toxicity (T) of chemicals (Escher et al., 2023) as regulated under REACH by the European Chemicals Agency (ECHA). Our recent findings, along with prior studies, demonstrate high tissue and cellular persistence and bioaccumulation, meeting criteria for classification of the studied particles as substances of concern.

7. Conclusion

Our study provides a comprehensive understanding of the interaction between PS-MNPs of sizes 0.25 and 1 μm and human colorectal cancer cell lines, highlighting the dependency on concentration, time, particle size, and cell type in both 2D and 3D cell cultures. We could clearly show that the particles are internalized *via* an energy-dependent endocytic pathway and that the particles were found mainly colocalized with lysosomes and to a lesser extent with endosomes in HCT116 cells. The particles exhibited high persistence in both monolayer and spheroid cultures, accumulating in the non-proliferating parts of multicellular spheroids. Despite their presence, no interruption of cell proliferation or division was observed. Importantly, particles were distributed between mother and daughter cells during division, with no signs of elimination. Moreover, our study reveals that particles smaller than 1 μm can enhance cell migration, potentially promoting metastasis. This observation aligns with recent research suggesting that MNPs can influence cellular behavior and potentially contribute to disease progression. Our study indicates the persistency and bioaccumulation of MNPs once accumulated in colorectal cancer cell lines, which are two out of three characteristics in toxicology and under the REACH regulation for potentially harmful chemicals.

Funding statement

MicroONE is a COMET Modul under the lead of CBmed GmbH (Graz, Austria; www.cbmed.at) within the COMET – Competence Centers for Excellent Technologies – programme, funded by the federal ministries BMK and BMAW, as well as the provinces of Styria and Vienna, and managed by the Austrian Research Promotion Agency (FFG; www.ffg.at/en). L.K. acknowledges financial support from the Austrian Federal Ministry of Science, Research and Economy, the National Foundation for Research, Technology and Development, and the Christian Doppler Research Association, as well as Siemens Healthineers. L.K. was also supported by a European Union Horizon 2020 Marie Sklodowska-Curie Doctoral Network grants (ALKATRAS, n. 675712; FANTOM, n. P101072735 and eRaDicate, n. 101119427) as well as BM Fonds (n. 15142), the Margaretha Hehberger Stiftung (n. 15142), the Christian-Doppler Lab for Applied Metabolomics (CDL-AM), and the Austrian Science Fund (grants FWF: P26011, P29251, P 34781 as well as the International PhD Program in Translational Oncology IPPTO 59.doc. funds). Additionally, this research was funded by the Vienna Science and Technology Fund (WWTF), grant number LS19-018. L.K. is a member of the European Research Initiative for ALK-Related Malignancies (www.erialcl.net). Open access funding provided by University of Vienna.

CRediT authorship contribution statement

Ekaterina Brynzak-Schreiber: Writing – review & editing, Writing – original draft, Supervision, Methodology, Formal analysis, Data curation. **Elisabeth Schögl:** Writing – review & editing, Methodology, Investigation, Data curation. **Carolin Bapp:** Writing – review & editing, Methodology, Investigation, Formal analysis, Data curation. **Klaudia Cseh:** Writing – review & editing, Supervision, Methodology, Formal analysis, Data curation. **Verena Kopatz:** Writing – review & editing, Methodology, Investigation, Formal analysis. **Michael A. Jakupec:** Writing – review & editing, Validation, Supervision, Methodology. **Andreas Weber:** Writing – review & editing, Validation, Supervision, Formal analysis. **Tobias Lange:** Writing – review & editing, Resources, Methodology, Investigation. **José L. Toca-Herrera:** Writing – review & editing, Supervision, Resources, Methodology. **Giorgia del Favero:** Writing – review & editing, Validation, Resources, Methodology. **Wolfgang Wadsak:** Writing – review & editing, Supervision, Resources, Project administration, Funding acquisition. **Lukas Kenner:** Writing – review & editing, Resources, Project administration, Funding acquisition. **Verena Pichler:** Writing – review & editing, Writing – original draft, Visualization, Validation, Supervision, Resources, Project administration, Methodology, Investigation, Formal analysis, Data curation, Conceptualization.

Declaration of competing interest

The authors declare that they have no known competing financial interests or personal relationships that could have appeared to influence the work reported in this paper.

Data availability

Data will be made available on request.

Acknowledgements

We thank A. Mohammed for support in initial experiments, C. Rademacher for the provision of the zetasizer Pro, A. Legin and E. Kiss for technical support. microONE is a COMET Modul under the lead of CBmed GmbH (Graz, Austria; www.cbmed.at) within the COMET – Competence Centers for Excellent Technologies – programme, funded by the federal ministries BMK and BMAW, as well as the provinces of Styria and Vienna, and managed by the Austrian Research Promotion Agency

(FFG; www.ffg.at/en).

Appendix A. Supplementary data

Supplementary data to this article can be found online at https://doi.org/10.1016/j.chemosphere.2024.141463.

References

Akhatova, F., Ishmukhametov, I., Fakhrullina, G., Fakhrullin, R., 2022. Nanomechanical atomic force microscopy to probe cellular microplastics uptake and distribution. Int. J. Mol. Sci. 23 (2), 806. https://doi.org/10.3390/ijms23020806.

Annangi, B., Villacorta, A., Vela, L., Tavakolpournegari, A., Marcos, R., Hernández, A., 2023. Effects of true-to-life PET nanoplastics using primary human nasal epithelial cells. Environ. Toxicol. Pharmacol. 100 https://doi.org/10.1016/j.etap.2023.104140.

Armistead, F.J., Gala De Pablo, J., Gadêlha, H., Peyman, S.A., Evans, S.D., 2020. Physical biomarkers of disease progression: on-chip monitoring of changes in mechanobiology of colorectal cancer cells. Sci. Rep. 10, 1–10. https://doi.org/10.1038/s41598-020-59952-x.

Banerjee, A., Billey, L.O., Shelver, W.L., 2021. Uptake and toxicity of polystyrene micro/nanoplastics in gastric cells: effects of particle size and surface functionalization. PLoS One 1–25. https://doi.org/10.1371/journal.pone.0260803.

Barguilla, I., Domenech, J., Ballesteros, S., Rubio, L., Marcos, R., Hernández, A., 2022. Long-term exposure to nanoplastics alters molecular and functional traits related to the carcinogenic process. J.l Hazard. Mater., 129470 https://doi.org/10.1016/j.jhazmat.2022.129470.

Bhattacharjee, S., 2016. DLS and zeta potential - what they are and what they are not? J. Contol. Release 337–351. https://doi.org/10.1016/j.jconrel.2016.06.017.

Brachner, A., Fragouli, D., Duarte, I.F., Farias, P.M.A., Dembski, S., Ghosh, M., Barisic, I., Zdzieblo, D., Vanoirbeek, J., Schwabl, P., Neuhaus, W., 2020. Assessment of human health risks posed by nano-and microplastics is currently not feasible. Int. J. Environ. Res. Public Health 1–10. https://doi.org/10.3390/ijerph17238832.

Brill-Karniely, Y., Dror, D., Duanis-Assaf, T., Goldstein, Y., Schwob, O., Millo, T., Orehov, N., Stern, T., Jaber, M., Loyfer, N., Vosk-Artzi, M., Benyamini, H., Bielenberg, D., Kaplan, T., Buganim, Y., Reches, M., Benny, O., 2020. Triangular correlation (TrC) between cancer aggressiveness, cell uptake capability, and cell deformability. Sci. Adv. https://doi.org/10.1126/sciadv.aax2861 eaax2861.

Bruinink, A., Wang, J., Wick, P., 2015. Effect of particle agglomeration in nanotoxicology. Arch. Toxicol. 659–675. https://doi.org/10.1007/s00204-015-1460-6.

Cassano, D., Bogni, A., La Spina, R., Gilliland, D., Ponti, J., 2023. Investigating the cellular uptake of model nanoplastics by single-cell ICP-MS. Nanomaterials 594. https://doi.org/10.3390/nano13030594.

Chamas, A., Moon, H., Zheng, J., Qiu, Y., Tabassum, T., Jang, J.H., Abu-Omar, M., Scott, S.L., Suh, S., 2020. Degradation rates of plastics in the environment. ACS Sustain. Chem. Eng. 3494–3511. https://doi.org/10.1021/acssuschemeng.9b06635.

Chang, Y.N., Liang, Y., Xia, S., Bai, X., Zhang, J., Kong, J., Chen, K., Li, J., Xing, G., 2020. The high permeability of nanocarriers crossing the enterocyte layer by regulation of the surface zonal pattern. Molecules 919. https://doi.org/10.3390/molecules25040919.

Ding, J., Huang, Y., Liu, S., Zhang, S., Zou, H., Wang, Z., Zhu, W., Geng, J., 2020. Toxicological effects of nano- and micro-polystyrene plastics on red tilapia: are larger plastic particles more harmless? J. Hazard. Mat., 122693 https://doi.org/10.1016/j.jhazmat.2020.122693.

Ershov, D., Phan, M.S., Pylvänäinen, J.W., Rigaud, S.U., Le Blanc, L., Charles-Orszag, A., Conway, J.R.W., Laine, R.F., Roy, N.H., Bonazzi, D., Duménil, G., Jacquemet, G., Tinevez, J.Y., 2022. TrackMate 7: integrating state-of-the-art segmentation algorithms into tracking pipelines. Nat. Methods 829–832. https://doi.org/10.1038/s41592-022-01507-1.

Escher, B.I., Altenburger, R., Blüher, M., Colbourne, J.K., Ebinghaus, R., Fantke, P., Hein, M., Köck, W., Kümmerer, K., Leipold, S., Li, X., Scheringer, M., Scholz, S., Schloter, M., Schweizer, P.J., Tal, T., Tetko, I., Traidl-Hoffmann, C., Wick, L.Y., Fenner, K., 2023. Modernizing persistence–bioaccumulation–toxicity (PBT) assessment with high throughput animal-free methods. Arch. Toxicol. 1267–1283. https://doi.org/10.1007/s00204-023-03485-5.

Firdessa, R., Oelschlaeger, T.A., Moll, H., 2014. Identification of multiple cellular uptake pathways of polystyrene nanoparticles and factors affecting the uptake: relevance for drug delivery systems. Eur. J. Cell Biol. 323–337. https://doi.org/10.1016/j.ejcb.2014.08.001.

Foroozandeh, P., Aziz, A.A., 2018. Insight into cellular uptake and intracellular trafficking of nanoparticles. Nanoscale Res. Lett. 339 https://doi.org/10.1186/s11671-018-2728-6.

Foty, R., 2011. A simple hanging drop cell culture protocol for generation of 3D spheroids. JoVE 20 (51), 4–7. https://doi.org/10.3791/2720.

Fröhlich, E., Meindl, C., Roblegg, E., Ebner, B., Absenger, M., Pieber, T.R., 2012. Action of polystyrene nanoparticles of different sizes on lysosomal function and integrity. Part. Fibre Toxicol. 1 https://doi.org/10.1186/1743-8977-9-26.

Gerashchenko, T.S., Novikov, N.M., Krakhmal, N.V., Zolotaryova, S.Y., Zavyalova, M.V., Cherdyntseva, N.V., Denisov, E.V., Perelmuter, V.M., 2019. Markers of cancer cell invasion: are they good enough? J. Clin. Med. 1–18. https://doi.org/10.3390/jcm8081092.

Ghoneum, M., Gollapudi, S., 2004. Phagocytosis of Candida albicans by metastatic and non metastatic human breast cancer cell lines in vitro. Cancer Detect. Prev. 17–26. https://doi.org/10.1016/j.cdp.2003.10.001.

Gigault, J., Halle, A. ter, Baudrimont, M., Pascal, P.Y., Gauffre, F., Phi, T.L., El Hadri, H., Grassl, B., Reynaud, S., 2018. Current opinion: what is a nanoplastic? Environ. Pollut. 1030–1034. https://doi.org/10.1016/j.envpol.2018.01.024.

Gonçalves, J.M., Sousa, V.S., Teixeira, M.R., Bebianno, M.J., 2022. Chronic toxicity of polystyrene nanoparticles in the marine mussel Mytilus galloprovincialis. Chemosphere 287 (September 2021), 132356. https://doi.org/10.1016/j.chemosphere.2021.132356.

Gruber, E.S., Stadlbauer, V., Pichler, V., Resch-Fauster, K., Todorovic, A., Meisel, T.C., Trawoeger, S., Hollóczki, O., Turner, S.D., Wadsak, W., Vethaak, A.D., Kenner, L., 2022. To waste or not to waste: questioning potential health risks of micro- and nanoplastics with a focus on their ingestion and potential carcinogenicity. Expo. Heal. 33–51. https://doi.org/10.1007/s12403-022-00470-8.

Guinney, J., Dienstmann, R., Wang, X., De Reyniès, A., Schlicker, A., Soneson, C., Marisa, L., Roepman, P., Nyamundanda, G., Angelino, P., Bot, B.M., Morris, J.S., Simon, I.M., Gerster, S., Fessler, E., De Sousa E Melo, F., Missiaglia, E., Ramay, H., Barras, D., et al., 2015. The consensus molecular subtypes of colorectal cancer. Nat Med 1350–1356. https://doi.org/10.1038/nm.3967.

Hartmann, N.B., Hüffer, T., Thompson, R.C., Hassellöv, M., Verschoor, A., Daugaard, A.E., Rist, S., Karlsson, T., Brennholt, N., Cole, M., Herrling, M.P., Hess, M.C., Ivleva, N.P., Lusher, A.L., Wagner, M., 2019. Are we speaking the same language? Recommendations for a definition and categorization framework for plastic debris. Environ. Sci. Technol. 1039–1047. https://doi.org/10.1021/acs.est.8b05297.

Hirschhaeuser, F., Menne, H., Dittfeld, C., West, J., Mueller-Klieser, W., Kunz-Schughart, L.A., 2010. Multicellular tumor spheroids: an underestimated tool is catching up again. J. Biotech. 3–15. https://doi.org/10.1016/j.jbiotec.2010.01.012.

Hwang, J., Choi, D., Han, S., Jung, S.Y., Choi, J., Hong, J., 2020. Potential toxicity of polystyrene microplastic particles. Sci. Rep. 1–12. https://doi.org/10.1038/s41598-020-64464-9.

Im, C., Kim, H., Zaheer, J., Kim, J.Y., Lee, Y.J., Kang, C.M., Kim, J.S., 2022. PET tracing of biodistribution for orally administered 64Cu-labeled polystyrene in mice. J. Nuc. Med. 461–467. https://doi.org/10.2967/JNUMED.120.256982.

Keinänen, O., Dayts, E.J., Rodriguez, C., Sarrett, S.M., Brennan, J.M., Sarparanta, M., Zeglis, B.M., 2021. Harnessing PET to track micro- and nanoplastics in vivo. Sci. Rep. 1–12. https://doi.org/10.1038/s41598-021-90929-6.

Kopatz, V., Wen, K., Kovács, T., Keimowitz, A.S., Pichler, V., Widder, J., Vethaak, A.D., Hollóczki, O., Kenner, L., 2023. Micro- and nanoplastics breach the blood–brain barrier (BBB): biomolecular corona's role revealed. Nanomaterials 1–10. https://doi.org/10.3390/nano13081404.

Kuhn, D.A., Vanhecke, D., Michen, B., Blank, F., Gehr, P., Petri-Fink, A., Rothen-Rutishauser, B., 2014. Different endocytotic uptake mechanisms for nanoparticles in epithelial cells and macrophages. Beilstein J. Nanotechn. 1625–1636. https://doi.org/10.3762/bjnano.5.174.

Li, Yanting, Shi, T., Li, X., Sun, H., Xia, X., Ji, X., Zhang, J., Liu, M., Lin, Y., Zhang, R., Zheng, Y., Tang, J., 2022a. Inhaled tire-wear microplastic particles induced pulmonary fibrotic injury via epithelial cytoskeleton rearrangement. Environ. Int., 107257 https://doi.org/10.1016/j.envint.2022.107257.

Li, Yuqi, Xu, M., Zhang, Z., Halimu, G., Li, Y., Li, Y., Gu, W., Zhang, B., Wang, X., 2022b. In vitro study on the toxicity of nanoplastics with different charges to murine splenic lymphocytes. J. Hazard. Mat., 127508 https://doi.org/10.1016/j.jhazmat.2021.127508.

Liu, Y.Y., Liu, J., Wu, H., Zhang, Q., Tang, X.R., Li, D., Li, C.S., Liu, Y., Cao, A., Wang, H., 2023. Endocytosis, distribution, and exocytosis of polystyrene nanoparticles in human lung cells. Nanomaterials 84. https://doi.org/10.3390/nano13010084.

Magrì, D., Veronesi, M., Sánchez-Moreno, P., Tolardo, V., Bandiera, T., Pompa, P.P., Athanassiou, A., Fragouli, D., 2021. PET nanoplastics interactions with water contaminants and their impact on human cells. Environ. Pollut. 271 https://doi.org/10.1016/j.envpol.2020.116262.

Martens, T.F., Remaut, K., Demeester, J., De Smedt, S.C., Braeckmans, K., 2014. Intracellular delivery of nanomaterials: how to catch endosomal escape in the act. Nano Today 9 (3), 344–364. https://doi.org/10.1016/j.nantod.2014.04.011.

Mohanan, N., Montazer, Z., Sharma, P.K., Levin, D.B., 2020. Microbial and enzymatic degradation of synthetic plastics. Front. Microbiol., 580709 https://doi.org/10.3389/fmicb.2020.580709.

Novikov, N.M., Zolotaryova, S.Y., Gautreau, A.M., Denisov, E.V., 2021. Mutational drivers of cancer cell migration and invasion. Br. J. Cancer 102–114. https://doi.org/10.1038/s41416-020-01149-0.

Schwabl, P., Koppel, S., Konigshofer, P., Bucsics, T., Trauner, M., Reiberger, T., Liebmann, B., 2019. Detection of various microplastics in human stool: a prospective case series. Ann. Int. Med. 453–457. https://doi.org/10.7326/M19-0618.

Schwarzfischer, M., Niechcial, A., Lee, S.S., Sinnet, B., Wawrzyniak, M., Laimbacher, A., Atrott, K., Manzini, R., Morsy, Y., Häfliger, J., Lang, S., Rogler, G., Kaegi, R., Scharl, M., Spalinger, M.R., 2022. Ingested nano- and microsized polystyrene particles surpass the intestinal barrier and accumulate in the body. NanoImpact 25. https://doi.org/10.1016/j.impact.2021.100374.

Sobhani, Z., Panneerselvan, L., Fang, C., Naidu, R., Megharaj, M., 2021. Chronic and transgenerational effects of polystyrene microplastics at environmentally relevant concentrations in earthworms (Eisenia fetida). Environ. Toxicol. Chem. 2240–2246. https://doi.org/10.1002/etc.5072.

Sorensen, R.M., Kanwar, R.S., Jovanovi, B., 2023. Past, present, and possible future policies on plastic use in the United States, particularly microplastics and nanoplastics: a review. Integr. Environ. Assess. Manag. 474–488. https://doi.org/10.1002/ieam.4678.

Stock, V., Böhmert, L., Lisicki, E., Block, R., Cara-Carmona, J., Pack, L.K., Selb, R., Lichtenstein, D., Voss, L., Henderson, C.J., Zabinsky, E., Sieg, H., Braeuning, A., Lampen, A., 2019. Uptake and effects of orally ingested polystyrene microplastic particles in vitro and in vivo. Arch. Toxicol. 1817–1833. https://doi.org/10.1007/s00204-019-02478-7.

Sutherland, R.M., 1988. Cell and enrivonment ineractions in tumor microregions : the spheroid model. Science 240, 177–184.

Turku Bioscience, n.d.retrieved february 28, 2024 https://bioscience.fi/services/cell-imaging/flowing-software/.

Vecchiotti, G., Colafarina, S., Aloisi, M., Zarivi, O., Di Carlo, P., Poma, A., 2021. Genotoxicity and oxidative stress induction by polystyrene nanoparticles in the colorectal cancer cell line HCT116. PLoS One 16, 1–18. https://doi.org/10.1371/journal.pone.0255120.

Villacorta, A., Rubio, L., Alaraby, M., López-Mesas, M., Fuentes-Cebrian, V., Moriones, O. H., Marcos, R., Hernández, A., 2022. A new source of representative secondary PET nanoplastics. Obtention, characterization, and hazard evaluation. J. Hazard. Mat. 439 https://doi.org/10.1016/j.jhazmat.2022.129593.

Ware, M.J., Colbert, K., Keshishian, V., Ho, J., Corr, S.J., Curley, S.A., Godin, B., 2016. Generation of homogenous three-dimensional pancreatic cancer cell spheroids using an improved hanging drop technique. Tissue Eng. - Part C: Methods 22, 312–321. https://doi.org/10.1089/ten.tec.2015.0280.

Xu, D., Ma, Y., Han, X., Chen, Y., 2021. Systematic toxicity evaluation of polystyrene nanoplastics on mice and molecular mechanism investigation about their internalization into Caco-2 cells. J.f Hazard. Mater. 417, 126092 https://doi.org/10.1016/j.jhazmat.2021.126092.

Xu, M., Halimu, G., Zhang, Q., Song, Y., Fu, X., Li, Y., Li, Y., Zhang, H., 2019. Internalization and toxicity: a preliminary study of effects of nanoplastic particles on human lung epithelial cell. Sci. Total Environ. 694, 133794 https://doi.org/10.1016/j.scitotenv.2019.133794.

Yong, C.Q.Y., Valiyaveettil, S., Tang, B.L., 2020. Toxicity of microplastics and nanoplastics in Mammalian systems. Int. J. Environ. Res. Public Health 17, 1509. https://doi.org/10.3390/ijerph17051509.

Zauner, W., Farrow, N.A., Haines, A.M.R., 2001. In vitro uptake of polystyrene microspheres: effect of particle size, cell line and cell density. J. Control. Release 71, 39–51. https://doi.org/10.1016/S0168-3659(00)00358-8.

Zhang, H., Zhang, S., Duan, Z., Wang, L., 2022. Pulmonary toxicology assessment of polyethylene terephthalate nanoplastic particles in vitro. Environ. Int. 162, 107177 https://doi.org/10.1016/j.envint.2022.107177.